Journal of
Micro/Nanolithography,
MEMS, and MOEMS

SPIEDigitalLibrary.org/jm3

Stochastic exposure kinetics of extreme ultraviolet photoresists: simulation study

Chris A. Mack
James W. Thackeray
John J. Biafore
Mark D. Smith

SPIE

Stochastic exposure kinetics of extreme ultraviolet photoresists: simulation study

Chris A. Mack
Lithoguru.com
1605 Watchhill Road
Austin, Texas 78703

James W. Thackeray
Dow Advanced Materials
455 Forest Street
Marlborough, Massachusetts 01752

John J. Biafore
Mark D. Smith
KLA-Tencor
FINLE Division
8843 N. Capital of Texas Highway
Austin, Texas 78759

Abstract. The stochastic nature of extreme ultraviolet (EUV) resist exposure leads to variations in the resulting acid concentration, which leads to line-edge roughness (LER) of the resulting features. Using a stochastic resist simulator, we predicted the mean and standard deviation of the acid concentration for an open-frame exposure and fit the results to analytical expressions. The EUV resist exposure mechanism of the PROLTIH Stochastic Resist Simulator is first order, and an analytical expression for the exposure rate constant C allows prediction of the mean acid concentration of an open-frame exposure to about 1% accuracy over a wide range of parameter values. A second analytical expression for the standard deviation of the acid concentration also matched the output of the simulator to within about 1%. Given the assumptions of the PROLTIH Stochastic Resist Simulator, it is possible to use the results of this paper to predict the stochastic uncertainty in acid concentration for EUV resists, thus allowing optimization of resist processing and formulations and contributing to a comprehensive LER model. [DOI: 10.1117/1.3631753]

Subject terms: stochastic modeling; extreme ultraviolet photoresist; exposure kinetics; line-edge roughness; linewidth roughness.

Paper 11033PRR received Mar. 23, 2011; revised manuscript received Aug. 1, 2011; accepted for publication Aug. 11, 2011; published online Sep. 19, 2011.

1 Introduction

Unlike the direct photon absorption mechanism of exposure for 248 and 193 nm photoresists, extreme ultraviolet (EUV) resists are exposed via photoionization: a high-energy photon absorbed in the resist ionizes the polymer, generating an electron (called a photoelectron), which in turn can generate several secondary electrons.[1] These electrons then scatter through the resist losing energy and, occasionally, interact with a photoacid generator (PAG) to generate an acid. Monte Carlo simulation of these events leads to a prediction of acid concentration as a function of exposure dose for a given set of resist parameters. Repeated simulations lead to prediction of both the mean and the standard deviation of the acid concentration. Both results are important in understanding EUV exposure kinetics and in predicting the impact of the kinetics on the line-edge and linewidth roughness of final lithographic images.

A common approach to studying line-edge roughness (LER) formation is through the use of Monte Carlo simulations[2–4] and mesoscale modeling.[5,6] In this paper an exposure simulator using a Monte Carlo statistical-mechanical technique called the PROLITH Stochastic Resist Model (SRM) (version X3.2, from KLA-Tencor) is used to model both the mean and standard deviation of the acid concentration after exposure for the simple case of a large open-frame exposure. By finding the mean acid concentration as a function of exposure dose, the exposure rate constant for an EUV resist is extracted as a function of the stochastic resist parameters. A semiempirical expression is developed that relates the value of this rate constant to the PROLITH resist parameters. Further, these same simulations yield the standard deviation of the acid concentration, which is compared to a proposed theoretical expression. Based on these results, a comprehensive approach to reducing the relative uncertainty in the after-exposure acid concentration of an EUV resist is provided.

2 Measuring *C*–193-nm Resist Test Case

For a continuum lithography model, the exposure rate constant C is either a direct input to the model (one of the Dill ABC parameters[7]), or is easily calculated from other input parameters such as the molar absorptivity and quantum efficiency of the PAG.[8] For a stochastic model, this is not necessarily the case. As we shall see below, the exposure model used by the PROLITH SRM for EUV resists does not have a first-order rate constant as an input, and in fact, it is not entirely clear that the exposure mechanism for an EUV resist will be first order (where the rate of acid generation is proportional to the remaining PAG concentration). Thus, a method is needed for determining if a simulator's overall mechanism for generating acid from exposure is first order, and if so, what the exposure rate constant is.

Fortunately, a simple test case allows for developing and testing a method for extracting C from a stochastic simulator. For 193 nm resists, the exposure model in the PROLITH SRM is based on the standard photochemical mechanism of direct absorption of the photon by the PAG. This means that the relationship between the inputs to the SRM [the base-10 molar absorptivity (molar extinction coefficient) ε and the quantum efficiency ϕ] and the C parameter should hold, as long as the results are averaged over a large number of photon

1932-5150/2011/$25.00 © 2011 SPIE

Table 1 Stochastic resist parameters for 193 nm simulations.

Exposure rate constant	0.024741 cm^2/mJ
Initial PAG density	0.05 nm^3
Absorption coefficient α	0.0015 nm^{-1}
Open frame area	50 nm × 50 nm
Resist thickness	50 nm
Exposure dose range	1 to 100 mJ/cm^2
Exposure dose steps	1 mJ/cm^2
Number of trials per dose	100

absorption events:

$$C = \phi \frac{2.303\varepsilon}{N_A}\left(\frac{\lambda}{hc}\right), \tag{1}$$

where h is Planck's constant, c is the vacuum speed of light, λ is the vacuum wavelength, and N_A is Avogadro's number. Thus, after developing and applying the method for extracting C from the stochastic simulation output, we can compare the results to the calculated value of C from Eq. (1) to check the efficacy and accuracy of the method. Note that the resist absorption coefficient is the (base e) molar absorptivity times the concentration of the absorbing species.

The PROLITH SRM has as an output the total number of acids generated during exposure in a preset simulation volume. Thus, the approach used here will be to simulate the exposure of an open frame and determine the number of acids generated as a function of exposure. To simplify the interpretation of the results, the resist, substrate, and immersion fluid will all be set to have the same refractive index as the resist so that no reflections will occur. This is not strictly possible in PROLITH since the immersion fluid must be nonabsorbing (the imaginary part of its refractive index is fixed at 0), but the impact of this tiny mismatch in refractive index is entirely negligible (reflectivity $= \kappa^2/4 \approx 0.01\%$ for a typical resist, where κ is the imaginary part of the resist refractive index). To eliminate radiometric effects, the reduction ratio for the simulation is set to 1 and coherent illumination is used so that all light is normally incident on the resist. The grid size for all simulations is set to 1 nm. The remaining simulation parameters for this 193 nm test case are shown in Table 1.

For any given exposure dose, the number of acids generated in the volume of resist is calculated by the SRM. An example output is shown in Figure 1. Since each data point is the output of a randomized (Monte Carlo) physical simulation of many photon absorption and exposure events, the size of the resist volume has a large impact on the stochastic "noise" of the results. This stochastic uncertainty can be further averaged out by repeating simulations (called trials) at each dose. For most of the results presented here, 100 trials per dose were run and the average number of photoacids over the trials was used. This average number of photoacids (n_{acid}) is then converted into an average relative acid concentration (h_{AVG}) by

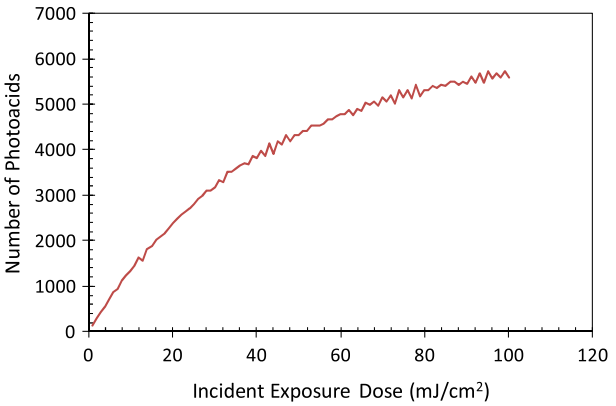

Fig. 1 Monte Carlo simulation of the number of photoacids generated during 193 nm exposure of a 50×50×50 nm resist volume as a function of exposure dose.

$$h_{\text{AVG}} = \frac{n_{\text{acid}}}{\rho_{\text{PAG}} V}, \tag{2}$$

where ρ_{PAG} is the initial PAG density and V is the simulation volume.

For a first-order exposure mechanism, the relative acid concentration is related to the incident exposure dose E_i by

$$-\ln(1 - h_{\text{AVG}}) \approx C E_{\text{AVG}}, \tag{3}$$

where

$$E_{\text{AVG}} = \frac{1}{D}\int_0^D E_i e^{-\alpha z} dz = E_i\left(\frac{1 - e^{-\alpha D}}{\alpha D}\right), \tag{4}$$

and α is the resist absorption coefficient and D is the resist thickness. The linear relationship in Eq. (3) is only approximate due to the nonlinear effect of absorption through the thickness of the resist. However, for a thin enough resist this linear approximation is a good one, and so will be used throughout this paper.

Figure 2 shows an example simulation for the 193 nm resist test case with 100 trials per exposure dose. The input values of PAG molar absorptivity and quantum efficiency give a value of C of 0.024741 cm^2/mJ and, in this simulation, the extracted slope was 0.024736 cm^2/mJ with a standard error of the slope equal to 1.0×10^{-5} cm^2/mJ

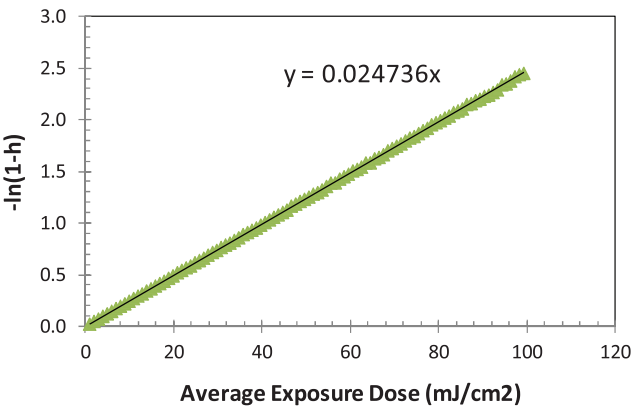

Fig. 2 Measurement of the exposure rate constant C as the slope of the line in this plot (data generated by the PROLITH SRM for a 193 nm resist).

(0.041%). Repeating this simulation experiment 20 times, the mean value of C was 0.0247381 cm^2/mJ with a standard deviation of 1.1×10^{-5} cm^2/mJ (0.045%), and a standard error of the mean equal to 2.5×10^{-6} cm^2/mJ (0.014%). The standard error of the slope is approximately equal to the standard deviation of the extracted value of C, with no statistically significant deviation from the true value of C. Thus, this method provides a reliable value for the first-order exposure rate constant C from Monte Carlo simulations of exposure.

3 Measuring *C*–Stochastic EUV Resist Model

The stochastic EUV resist model of the PROLITH SRM does not assume a first-order exposure model *per se*, but instead simulates a sequence of more elementary steps that lead to the generation of an acid.[9] Photons originating from the projection optics impinge upon the resist film. The number of photons absorbed by the resist is determined by Lambert's law and Poisson statistics (in this study, the PAG is assumed to not directly absorb photons). Once a photon has been absorbed, one electron is (possibly) released with probability ϕ_e, and with kinetic energy equal to the photon energy minus the ionization potential, IP. This photoelectron (or primary electron) then travels and scatters through the resist, possibly inducing further ionization and resulting in a secondary electron cascade. The interaction of scattering electrons with the resist involves (at least) elastic and inelastic collisions: in an elastic collision the resist is left in the original state; in an inelastic collision the resist is ionized and a secondary electron ejected. Other inelastic events, such as phonon generation, can also be modeled,[10] but they have not been included in the current model. As the electrons travel through the resist, they lose kinetic energy continuously (in a continuous slowing-down approximation). The stopping power of the resist is the energy lost by an electron per path length traveled and is calculated with the complex dielectric function for a model compound (polystyrene, C_8H_8). Photoacid generators are randomly dispersed throughout the resist with average density ρ_{PAG}. Electrons traveling within the reaction radii (r) of PAGs may be of energy sufficient to produce excitation (PAG excitation energy, E_{excit}). This approach is based on the interaction radius commonly used to describe diffusion-controlled reaction kinetics in condensed media (see, for example, Refs. 1, 11, and 12) combined with the energy transferred to the resist via the stopping power. A different approach, based on a virtual photon, has been described by Han and Cerrina.[13] Both approaches assume that the probability that a PAG will be electronically excited depends on both the energy of the electron and the minimum electron-PAG distance. PAGs in an electronically-excited state are converted to acid with a probability given by the PAG quantum efficiency (ϕ_{PAG}). Further details of this exposure model have been previously published.[9]

Thus, there are a large number of parameters that influence the generation of an acid or acids for any given EUV photon incident on the resist. The baseline values of these parameters for the simulations in this paper are given in Table 2. As various parameter values were changed in the studies presented below, the exposure dose range was adjusted so that at the highest dose approximately 90% of the PAG was converted to acid.

Table 2 Stochastic resist parameters for EUV simulations.

PAG molar absorptivity	0
Initial PAG density, ρ_{PAG}	0.05 nm^3
Absorption coefficient, α	0.006516 nm^{-1}
Electron generation efficiency, ϕ_e	0.9
Ionization potential, IP	10 eV
PAG excitation radius, r	2.0 nm
PAG excitation energy, E_{excit}	5 eV
PAG quantum efficiency, ϕ_{PAG}	0.5
Open frame area	50 nm × 50 nm
Resist thickness	10 nm
Exposure dose range	0.25 to 25 mJ/cm^2
Exposure dose steps	0.25 mJ/cm^2
Number of trials per dose	100

In all of the studies presented below, the EUV stochastic resist model of PROLITH exhibited overall first-order exposure kinetics, so that the method for extracting C described in Sec. 2 could be applied. With 100 trials per exposure dose, the 95% confidence interval for a typical value of C is about $\pm 0.07\%$. Each of the parameters of the model were varied in order to understand their impact on C. As expected, PAG density did not affect the value of C. Other parameters were more interesting.

3.1 *Absorption Coefficient*

Since only an absorbed photon can generate photo- and secondary electrons and cause acid generation, one would expect a monotonic increase in C with absorption coefficient. The Lambert law of absorption essentially says that the absorption probability per unit length traveled is a constant, equal to the absorption coefficient of the material α. Since the model used here assumes that all absorption is done by the polymer, each absorption event is equally likely to result in a photoelectron. Thus, one expects to find that C is proportional to α. Figure 3 confirms this expectation. Since the resist thickness was fixed at 10 nm, a high absorption coefficient (> 0.01 nm^{-1}) produces a nonlinear effect through the resist thickness, and thus the deviation from linearity seen in Figure 3.

3.2 *Electron Generation Efficiency*

Given the model used here, one would expect that C would be directly proportional to the electron generation efficiency, ϕ_e. Simulation results confirm this prediction, as seen in Figure 4.

3.3 *Ionization Potential*

When photon absorption leads to the generation of a photoelectron, the resulting electron has initial kinetic energy

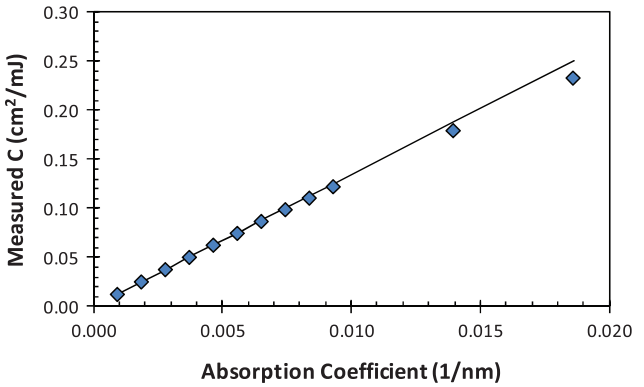

Fig. 3 Measurement of the EUV resist exposure rate constant *C* as a function of the resist absorption coefficient α.

equal to the photon energy minus the ionization potential, IP. Thus, higher ionization potential leads to a lower energy electron, which then has less energy available to find a PAG and cause photoacid generation. Simulations show that the impact of ionization potential can be well described by

$$C = C_0 \left(1 - \frac{\mathrm{IP}}{\mathrm{IP}_0}\right), \tag{5}$$

where C_0 is the value of C when $\mathrm{IP} = 0$, and IP_0 is the value of the ionization potential that makes $C = 0$. Thus, one expects IP_0 to be about equal to the photon energy (91.8 eV for an EUV photon) minus the PAG excitation energy. Figure 5 shows that Eq. (5) does fit the simulated results, but with the value of IP_0 dependent upon the mechanism for PAG reaction with the secondary electron. For these simulations, $\mathrm{IP}_0 = 103$ eV when the PAG reaction radius $r = 1$ nm, and $\mathrm{IP}_0 = 111$ eV when $r = 2$ nm.

The value of IP_0 extracted from these simulations as a function of the PAG reaction radius (with the PAG excitation energy fixed at 0.2 or 5 eV) is shown in Figure 6. Using the PAG reaction cross-section ($\sigma_{e\text{–PAG}}$, with units of nm^2) defined in Secs. 3.4 and 3.5, Figure 6(b) shows that IP_0 matches the expected value ($91.8\,\mathrm{eV} - E_{\mathrm{excit}}$) when the reaction cross-section goes to zero, and follows this empirical expression in general:

$$\mathrm{IP}_0 = 91.8\,\mathrm{eV} - E_{\mathrm{excit}} + 16.4\,(\sigma_{e-\mathrm{PAG}})^{0.15}. \tag{6}$$

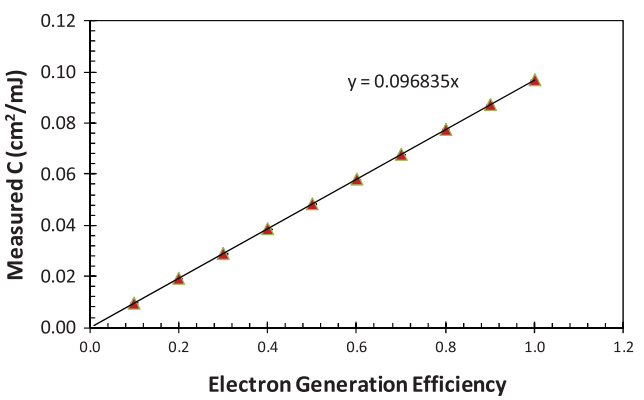

Fig. 4 Measurement of the EUV resist exposure rate constant *C* as a function of the electron generation efficiency ϕ_e.

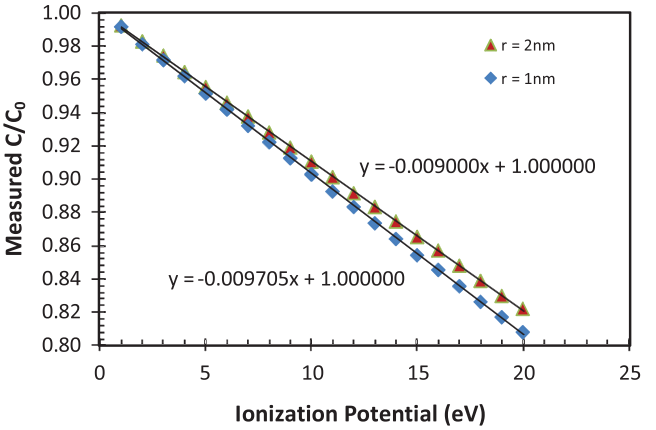

Fig. 5 Measurement of the EUV resist exposure rate constant *C* as a function of the ionization potential IP for two different values of the PAG reaction radius, *r*.

The physical meaning of this result is not clear. While Eq. (6) matches the simulated results quite well, the simpler approach of fixing the value of IP_0 to about 110 eV in Eq. (5) provides a reasonable estimation of the impact of ionization potential on C for a reasonable range of PAG reaction parameters.

3.4 *PAG Reaction Radius*

When an electron comes within the PAG reaction radius, r, of a (randomly positioned) PAG molecule, a reaction is possible. Thus, a larger PAG reaction radius is expected to yield a larger value of C. This concept, in fact, is the same as that of a reaction cross-section, where the reaction rate is proportional to the reaction cross-section, which in turn is proportional to the reaction radius squared. In the classical kinetic cross-section approach, all of the energy of the electron would be assumed to be transferred to the PAG during a collision. Here, the continuous slowing down approximation assumes that the traveling electron is losing energy per nanometer traveled to its environment. When the electron is within the reaction radius, the energy lost by the electron is transferred to the PAG. Only if the energy lost to the PAG is greater than the PAG excitation energy will there be a chance of generating an acid. This means there will be a minimum PAG reaction radius for reaction (r_0), below which even the most energetic electron will not be able to transfer enough of its energy to the PAG in order to overcome this excitation barrier. Thus, an expected behavior is

$$C \propto \sigma_{e-\mathrm{PAG}}, \quad \sigma_{e-\mathrm{PAG}} = \pi\,(r - r_0)^2, \tag{7}$$

where $\sigma_{e\text{–PAG}}$ is the electron-PAG reaction cross-section.

Figure 7 shows the simulation results for C as a function of PAG reaction radius, for two different PAG excitation energies (2.2 and 5.0 eV). The quadratic model fits the data very well, with r_0 a function of the PAG excitation energy (as will be discussed in Sec. 3.5).

3.5 *PAG Excitation Energy*

When energy is transferred from a secondary electron to a PAG molecule, the generation of an acid is possible only if the energy transferred exceeds a threshold value, called the PAG excitation energy, E_{excit}. As mentioned in Sec. 3.4,

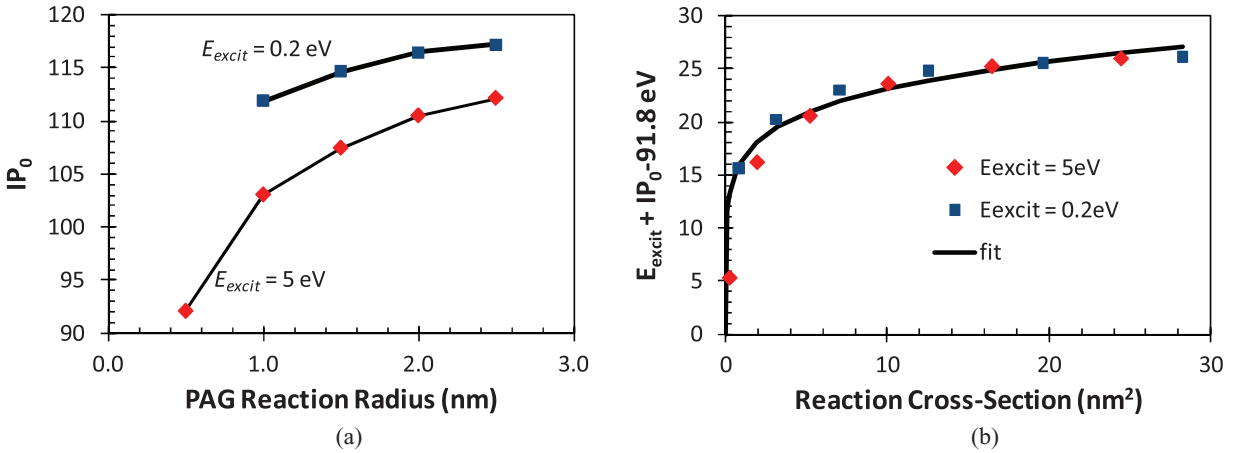

Fig. 6 (a) The extracted value of IP_0 as a function of the PAG reaction radius, r, for two different PAG excitation energies. (b) as a function of the PAG reaction cross-section.

simulations have shown that the impact of changing E_{excit} can be modeled as simply a change in the value of r_0. Figure 8(a) shows the simulation results for two different PAG reaction radii. For moderately low excitation energies (less than or equal to about 5 eV), the fall-off is approximately quadratic. In fact, data in this range of excitation energies can be well fitted by

$$r_0 = 0.0084 E_{\text{excit}}^2, \tag{8}$$

where r_0 is in nanometers and E_{excit} is in electron-volts. For higher excitation energies, a more complex model will be required [see Figure 8(b)].

3.6 *PAG Quantum Efficiency*

When a PAG molecule receives energy in excess of the required excitation energy, an acid is generated with probability equal to the PAG quantum efficiency, ϕ_{PAG}. At first thought, one would expect C to be linearly proportional to ϕ_{PAG}. Simulations (as given in Figure 9) show a more interesting behavior. As the quantum efficiency approaches 1, the impact on C begins to saturate: there is a smaller incremental increase in C for the same incremental increase in ϕ_{PAG}. Further reflection, however, makes the reason for this behavior clear.

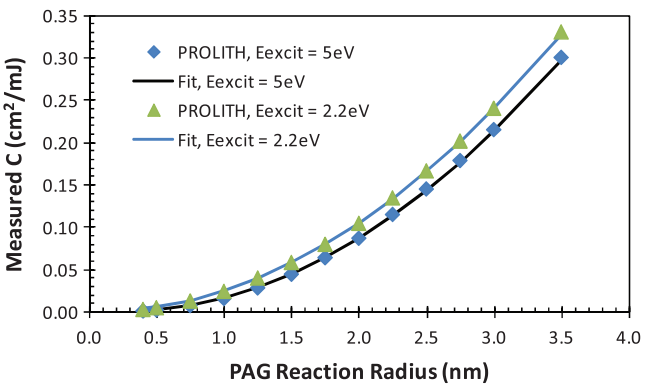

Fig. 7 Measurement of the EUV resist exposure rate constant C as a function of the PAG reaction radius for two different values of the PAG excitation energy, E_{excit}. Fit curves follow Eq. (7).

One of the most interesting aspects of an EUV resist is the possibility of an acid yield (the average number of generated acids per absorbed photon) greater than 1. Since the energy of one EUV photon (92 eV) far exceeds the minimum energy required to convert a PAG into an acid (on the order of 5 eV), each absorbed photon can potentially generate many acids. But for that to happen, there must be a sufficient number of unreacted PAGs in the neighborhood of the absorption event. Consider the initial (low-dose) acid yield, Y_0, defined as

$$Y_0 = \lim_{\text{dose}\to 0}\left(\frac{\#\,\text{acids}}{\#\,\text{absorbed photons}}\right). \tag{9}$$

From the definition of C, this initial acid yield will be

$$Y_0 = \frac{C}{\alpha}\left(\frac{hc}{\lambda}\right)\rho_{\text{PAG}}. \tag{10}$$

As the density of unreacted PAGs decreases with higher exposure doses, the acid yield must also decrease, leading to a saturation in how large C can be.

To quantify this saturation, let r_e be the maximum distance a secondary electron will travel from the point of photon absorption and still have sufficient energy to excite a PAG (note: this is not a hypothetical straight-line path for the electron; scattering is included in this maximum radius). The maximum number of PAGs that can possibly be converted by one absorbed photon is then the number of PAGs to be found in a sphere of this radius:

$$\text{Max}\,\#\,\text{acids} = \left(\frac{4}{3}\pi r_e^3\right)\rho_{\text{PAG}}. \tag{11}$$

The maximum possible acid yield occurs when the maximum number of acids are generated for each absorbed photon. This leads, then, to a maximum possible value of C, called C_{max}:

$$C_{\text{max}} = \left(\frac{4}{3}\pi r_e^3\right)\alpha\left(\frac{\lambda}{hc}\right). \tag{12}$$

Note that the maximum possible value of C does not depend on the initial PAG density. It depends entirely on the absorption coefficient and r_e, the maximum distance a secondary electron can travel and still have sufficient energy to excite a

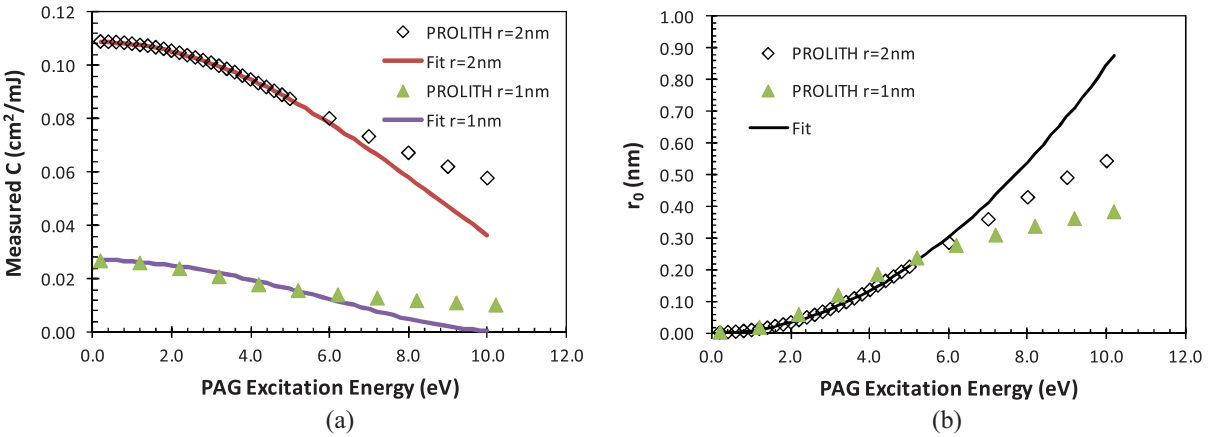

Fig. 8 Measurement of the EUV resist (a) exposure rate constant C, and (b) fitted model parameter r_0 as a function of the PAG excitation energy for two different values of the PAG reaction radius, r. For both graphs, the fit curves follow Eqs. (7) and (8).

PAG. The existence of $C_{\max}$ leads to the observed saturation of C as the PAG quantum efficiency grows. The observed nonlinear behavior seen in Figure 9 can now be fit with a semiempirical expression for this saturation:

$$C = C_{\max}\left(1 - e^{-\gamma\phi_{\mathrm{PAG}}}\right), \tag{13}$$

where γ determines the degree of nonlinearity. Fitting Eq. (13) to the simulated data of C versus ϕ_{PAG} allows both γ and $C_{\max}$ (and thus r_e) to be determined. Table 3 shows the results of such a fit for several sets of model input parameters. It is very interesting that this approach provides not only a model for the behavior of C with ϕ_{PAG}, but a way of extracting the "electron blur" of the model, the effective distance that photo- and secondary electrons travel while causing acid generation. For the range of model parameters investigated here, this electron blur radius is in the range of 2.1 to 3.3 nm.

3.7 *Overall Model for C*

Combining all of the observations described above, an analytical model for C based on the PROLITH EUV SRM can be established. For the case where the PAG excitation energy is about 5 eV or less, and the PAG quantum efficiency is low enough that the nonlinear saturation of Eq. (13) can be ignored,

$$C \approx d_0\left(1 - \frac{\mathrm{IP}}{110\,\mathrm{eV}}\right)\alpha\phi_e\phi_{\mathrm{PAG}}\sigma_{e-\mathrm{PAG}}\left(\frac{\lambda}{hc}\right), \tag{14}$$

where $\sigma_{e-\mathrm{PAG}} = \pi\,(r - r_0)^2$ and $r_0 = 0.0084E^2_{\mathrm{excit}}$, and where the constant d_0 is empirically determined to be 4.75 nm. [It is interesting to note that Eq. (14) is based on the results of well over one million open-frame stochastic exposure simulations.] Over a useful range of model input parameters, this semiempirical expression predicts the value of C obtained from the PROLITH Stochastic Resist Model version X3.2 to within about 1% to 2%. More complicated expressions are certainly possible if PAG excitation energies greater than 5 eV or PAG quantum efficiencies near 1 are to be used, or if a more accurate model for the impact of ionization potential is desired. It would also be interesting to discover what details of the electron scattering and energy loss model give rise to the specific values of the empirical constants observed here.

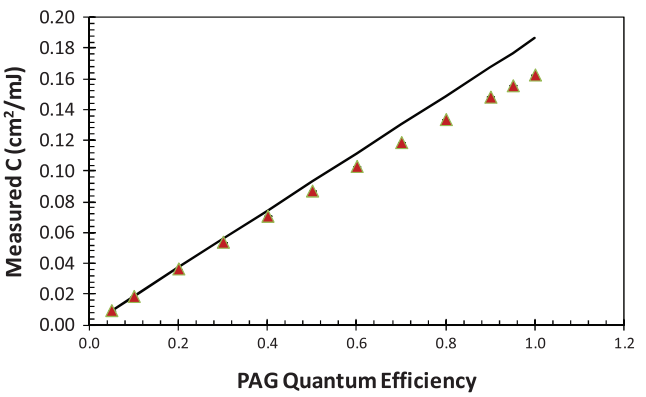

Fig. 9 Measurement of the EUV resist exposure rate constant C as a function of the PAG quantum efficiency. A straight line through the first few data points is shown for comparison.

3.8 *Theoretical Model for C*

Equation (14) is a semiempirical model that replicates the mean outcome of the PROLITH SRM with reasonable accuracy. Here, a simplified two-step mechanism for EUV exposure will lead to an analytical rate equation that can be compared to this semiempirical result. Consider first the generation of photoelectrons. Letting ρ_{pe} be the number density of photoelectrons generated by exposure, a standard kinetic rate equation for photoelectron generation will be similar to the standard rate equation for direct photon resist exposure:[14]

$$\frac{d\rho_{\mathrm{pe}}}{dt} = \alpha\phi_e I\left(\frac{\lambda}{hc}\right), \tag{15}$$

where I is the intensity of light. Solving this rate equation,

$$\rho_{\mathrm{pe}} = \alpha\phi_e E\left(\frac{\lambda}{hc}\right), \tag{16}$$

where E is the exposure dose.

Now, let these photoelectrons migrate through the resist, colliding with a PAG to generate an acid. A standard

Table 3 Impact of various model parameters on the saturation of the exposure rate constant.

Ionization potential (eV)	PAG excitation energy (eV)	PAG reaction radius (nm)	C_{max} (cm^2/mJ)	r_e (nm)	Nonlinear term γ
10	5	2	0.65	3.3	0.29
0.1	5	2	0.61	3.2	0.34
10	0.2	2	0.58	3.1	0.41
10	5	1	0.17	2.1	0.20

second-order rate equation based on collision kinetic theory would look like

$$\frac{d\rho_{\mathrm{PAG}}}{dt} = v\phi_{\mathrm{PAG}}\sigma_{e-\mathrm{PAG}}\rho_{\mathrm{pe}}\rho_{\mathrm{PAG}}, \tag{17}$$

where $\sigma_{e-\mathrm{PAG}}$ is the reaction cross-section between the electron and the PAG and v is the velocity of the electron. Note that t in this equation is the time the electron spends moving about the resist and reacting with PAGs. Combining Eqs. (16) and (17) and integrating,

$$\rho_{\mathrm{PAG}} = \rho_{\mathrm{PAG}-0}e^{-K}, \quad \text{where} \quad K = v\phi_{\mathrm{PAG}}\sigma_{e-\mathrm{PAG}}\int_0^\infty \rho_{\mathrm{pe}}dt. \tag{18}$$

Defining the lifetime τ of the photoelectron as

$$\tau = \frac{1}{\rho_{\mathrm{pe}}(t=0)}\int_0^\infty \rho_{\mathrm{pe}}dt, \tag{19}$$

and noting that the photoelectron density at $t = 0$ is given by Eq. (16), we have

$$K = \mathrm{CE} = \alpha\phi_e\phi_{\mathrm{PAG}}\sigma_{e-\mathrm{PAG}}E\left(\frac{\lambda}{hc}\right)v\tau. \tag{20}$$

Letting $d_e = v\tau$, this quantity can be thought of as the mean effective path length (an effective Bethe range) of the photoelectron traveling in the resist. If the photoelectron generates secondary electrons, then this distance can be interpreted as the mean sum of the path lengths of all the electrons. The final result is

$$C = d_e\phi_e\alpha\phi_{\mathrm{PAG}}\sigma_{e-\mathrm{PAG}}\left(\frac{\lambda}{hc}\right). \tag{21}$$

Comparing this theoretical expression for the overall exposure rate constant to the Eq. (14) fit to the results of the simulations, we see that they are identical when

$$d_e = d_0\left(1 - \frac{\mathrm{IP}}{110\,\mathrm{eV}}\right). \tag{22}$$

The empirically derived value of 4.75 nm for d_0 can now be interpreted as the mean electron path length in the resist for the limiting case of IP = 0. It is interesting to compare this value with the values of r_e determined earlier (~2 to 3 nm).

Thus, the simplified two-step kinetic exposure model presented in this section matches the overall results obtained from the more detailed mechanism embedded in the PROLITH SRM. Of course, the more detailed EUV exposure mechanism in PROLITH allows d_e and $\sigma_{e-\mathrm{PAG}}$ to be expressed as a function of more fundamental scattering and reaction parameters. Note also that a simplified mechanism where only one photoelectron reacts with PAGs does not alter the overall form of the expression for C compared with the case where a cascade of secondary electrons can react with the PAGs.

4 EUV Acid Fluctuations

Section 3 described an analytical model that could predict the average number of acids generated in a given volume as a function of exposure dose. From the perspective of LER, a more important term to predict is the standard deviation of the acid concentration. By simulating open frame exposures with the PROLITH SRM, this standard deviation can also be extracted.

For a 193 nm resist, the exposure mechanism is simple enough that an analytical expression for the standard deviation of the acid concentration can be derived.[15,16] Defining $\langle h\rangle$ as the mean concentration of acid relative to the initial concentration of unexposed PAG [essentially the same as h_{AVG} from Eq. (2)], the standard deviation of this acid concentration in some volume V will be σ_h, given by

$$\left(\frac{\sigma_h}{\langle h\rangle}\right)^2 = \frac{1}{\langle h\rangle\langle n_{0-\mathrm{PAG}}\rangle} + \left[\frac{(1-\langle h\rangle)\ln(1-\langle h\rangle)}{\langle h\rangle}\right]^2 \times \frac{1}{\langle n_{0-\mathrm{PAG}}\rangle\langle n_{\mathrm{photons}}\rangle}, \tag{23}$$

where $\langle n_{0-\mathrm{PAG}}\rangle = \rho_{\mathrm{PAG}}V$ is the mean number of PAGs initially found in that volume and $\langle n_{\mathrm{photons}}\rangle$ is the mean number of photons incident upon the top of the resist volume. This result is reasonably intuitive. The first term on the right-hand side of Eq. (23) is the expected Poisson result based on exposure kinetics–the relative uncertainty in the resulting acid concentration after exposure goes as one over the square root of the mean number of acid molecules generated within the volume of interest. For large volumes and reasonably large exposure doses, the number of acid molecules generated is large and the statistical uncertainty in the acid concentration becomes relatively small. For small volumes or low doses, a small number of photogenerated acid molecules results in a large relative uncertainty in the actual number within that volume. The second term accounts for photon shot noise and adds to the variance due to chemical concentration shot noise (making the final uncertainty worse than Poisson). For 193 nm resists, the impact of this photon shot noise term is minimal compared to variance in acid concentration caused by simple molecular position uncertainty. Unfortunately, the same is not true for EUV resists.

The second term on the right-hand side of Eq. (23) includes the product of the number of photons and the number of PAGs, the absorbing species. This product is an obvious consequence of the mechanism of exposure for 193 nm resists. For EUV resists, however, the entire resist is an absorption site, so that stochastic uncertainty is not limited by photons finding an appropriate absorption site. Instead, the stochastic limiter is the number of photoelectrons generated. Thus, by analogy with the result for 193 nm resists, an expected behavior for EUV resists would be

$$\left(\frac{\sigma_h}{\langle h\rangle}\right)^2 = \frac{1}{\langle h\rangle\langle n_{0-\mathrm{PAG}}\rangle} + \left[\frac{(1-\langle h\rangle)\ln(1-\langle h\rangle)}{\langle h\rangle}\right]^2 \times \frac{1}{\langle n_{\mathrm{photoelectrons}}\rangle}, \tag{24}$$

where

$$\langle n_{\mathrm{photoelectrons}}\rangle = \phi_e\langle n_{\mathrm{photons}}\rangle(1-e^{-\alpha D}),\ \ \langle h\rangle = 1-e^{-C\langle E_{\mathrm{AVG}}\rangle}$$

and $\langle n_{\mathrm{photoelectrons}}\rangle$ is the mean number of photoelectrons generated in the volume. It is expected that this equation can be derived directly from the simplified two-step exposure mechanism described in Sec. 3.

To test this hypothesis, the SRM was run over a range of parameters using the same open-frame exposure approach as described above for determining C. For each open-frame simulation, the number of acids found in the volume at the end of exposure is determined. Repeating the simulation many (typically 4,000 to 20,000) times, both the mean number of acids and the standard deviation are calculated. To get the best match to the simulated data (with residuals whose mean is near zero and with minimum variance), a slight modification to Eq. (24) was required:

$$\left(\frac{\sigma_h}{\langle h\rangle}\right)^2 = \frac{1}{\langle h\rangle\langle n_{0-\mathrm{PAG}}\rangle} + 1.07\left(\frac{(1-\langle h\rangle)\ln(1-\langle h\rangle)}{\langle h\rangle}\right)^2 \times \frac{1}{\langle n_{\mathrm{photoelectrons}}\rangle}. \tag{25}$$

The reason why the second term on the right-hand side of Eq. (25) had to increase by 7% in order to match the PROLITH SRM output is not clear. A typical result, using the nominal parameters of Table 2, is shown in Figure 10. The fit of this equation to the SRM simulated data is remarkably good.

To test the accuracy of Eq. (25), all of the EUV exposure model parameters were varied to determine their impact on the variance of the acid concentration. For the nominal case of Figure 10, the RMS error between PROLITH and the analytical expression is less than 0.5% over the range of exposure doses used. In Figure 11 the PAG quantum efficiency was varied (with the impact of changing C). The analytical model of Eq. (25) matches the SRM results extremely well for $\phi_{\mathrm{PAG}} = 0.25$, 0.5, and 1.0 (RMS errors between 1% and 2%). Further tests set the imaginary part of the resist refractive index κ to 0.004, 0.007, and 0.01; the photoelectron generation probability ϕ_e to 0.45 and 0.9; the ionization potential IP to 1, 10, and 20 eV; the PAG reaction radius r to 1, 2, and 3 nm; and the PAG excitation energy to 2 and 5 eV. In all cases, the analytical model of Eq. (25) matches the SRM results with this same level of accuracy (typical rms errors near 1%). Figure 12 shows the impact of varying the initial PAG density ρ_{PAG}, with values of 0.1, 0.2, and 0.4 nm^{-3}. Again, Eq. (25) matches the SRM results extremely well (rms errors below 1%).

An interesting simplification to Eq. (24) comes for the case of $\alpha D \ll 1$. For this case, the number of photoelectrons generated becomes

$$\langle n_{\mathrm{photoelectrons}}\rangle \approx \alpha D\phi_e\langle n_{\mathrm{photons}}\rangle = \alpha\phi_e E\left(\frac{\lambda}{hc}\right)V, \tag{26}$$

so that the ratio of the mean initial number of PAGs to the mean number of photoelectrons is

$$\frac{\langle n_{0-\mathrm{PAG}}\rangle}{\langle n_{\mathrm{photoelectrons}}\rangle} \approx \frac{\rho_{\mathrm{PAG}}}{\alpha\phi_e E\left(\frac{\lambda}{hc}\right)} = \left[\frac{C\left(\frac{hc}{\lambda}\right)}{\alpha\phi_e}\right]\left[\frac{\rho_{\mathrm{PAG}}}{-\ln(1-\langle h\rangle)}\right]. \tag{27}$$

Recalling the definition of initial acid yield from Eq. (10),

$$\frac{\langle n_{0-\mathrm{PAG}}\rangle}{\langle n_{\mathrm{photoelectrons}}\rangle} \approx \frac{-1}{\ln(1-\langle h\rangle)}\frac{Y_0}{\phi_e}. \tag{28}$$

Thus, Eq. (24) becomes

$$\left(\frac{\sigma_h}{\langle h\rangle}\right)^2 \approx \frac{1}{\langle h\rangle\langle n_{0-\mathrm{PAG}}\rangle}\left[1-\frac{(1-\langle h\rangle)^2\ln(1-\langle h\rangle)}{\langle h\rangle}\left(\frac{Y_0}{\phi_e}\right)\right]. \tag{29}$$

It is instructive to compare the magnitudes of the two terms on the right-hand side of Eq. (24). For the sake of clarity of discussion, we shall define

$$\text{Ideal acid shot noise} = \sqrt{\frac{1}{\langle h\rangle\langle n_{0-\mathrm{PAG}}\rangle}}$$

$$\text{Photoelectron shot noise} = \left|\frac{(1-\langle h\rangle)\ln(1-\langle h\rangle)}{\langle h\rangle}\right| \times \sqrt{\frac{1}{\langle n_{\mathrm{photoelectrons}}\rangle}}. \tag{30}$$

The relative acid uncertainty, $\sigma_h/\langle h\rangle$, is the square root of the sum of the squares of these two terms. As Figure 13 shows for the nominal case of Table 2, the Poisson acid shot noise dominates when $\langle h\rangle > 0.65$, and is limited by the initial PAG Poisson concentration uncertainty as $\langle h\rangle \to 1$. When $\langle h\rangle < 0.65$, the photoelectron term (which includes photon shot noise) dominates. The cross-over value of $\langle h\rangle$ (the value that makes the acid and photoelectron shot noise terms equal) is a function of the initial acid yield, and in the low-absorption limit [that is, using Eq. (29)] varies approximately as

$$\langle h\rangle_{\mathrm{crossover}} \approx 1-\left(\frac{\phi_e}{Y_0}\right)^{0.65}. \tag{31}$$

5 Discussion of Results

To model the mechanism of line-edge roughness formation in EUV resist, it is necessary to predict both the mean and the standard deviation of the acid concentration resulting from exposure. Microscopic stochastic simulators such as

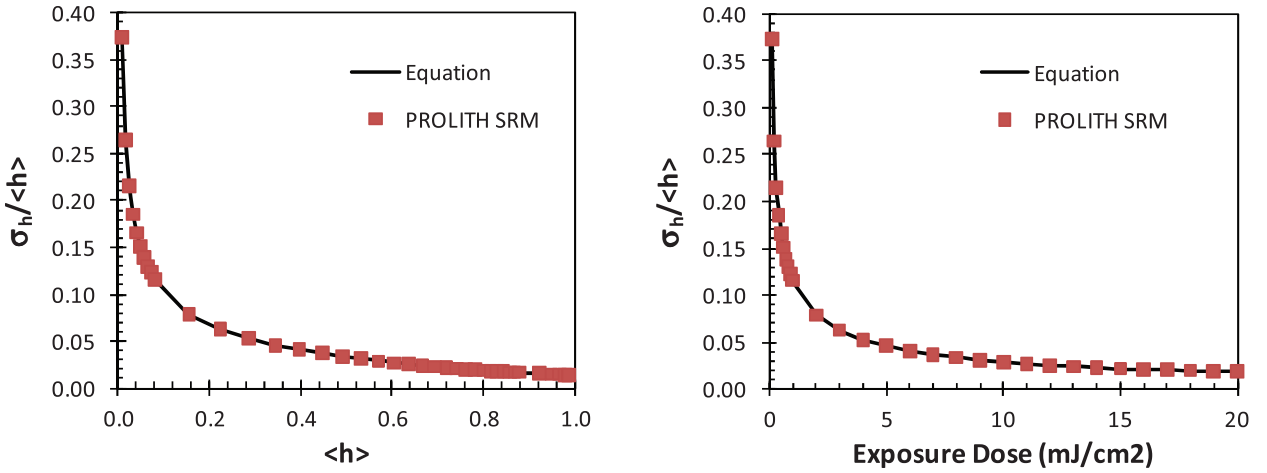

Fig. 10 Typical example (using the baseline parameters of Table 2, with $C = 0.08652\ \mathrm{cm}^2/\mathrm{mJ}$) of how the relative uncertainty in acid concentration varies with (a) the mean acid concentration, and (b) the incident exposure dose. Symbols give the PROLITH SRM simulation results, the solid line shows the prediction of Eq. (25).

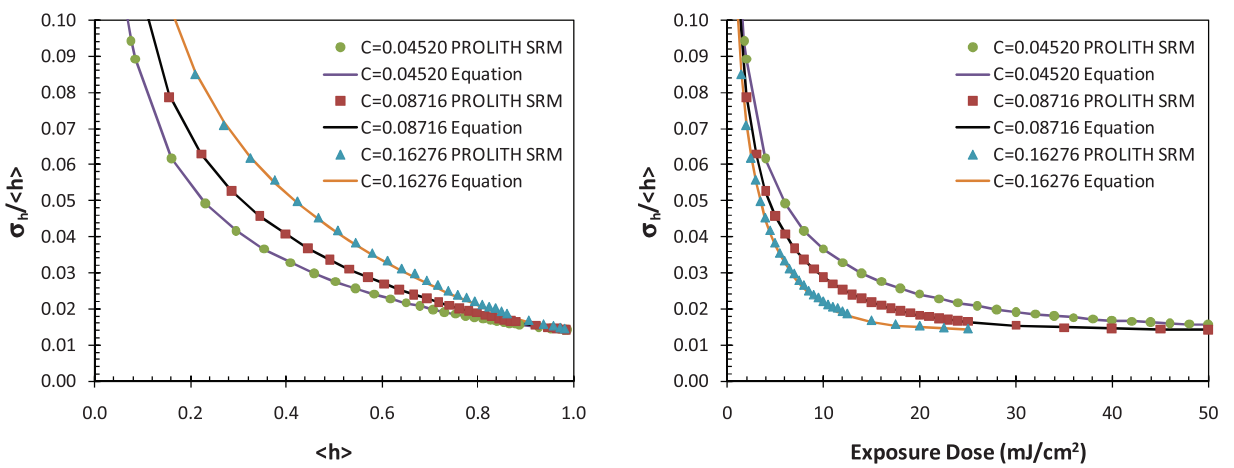

Fig. 11 Impact of PAG quantum efficiency (with values of 0.25, 0.5, and 1.0) on the relative uncertainty in acid concentration, shown as a function of mean relative acid concentration and of dose. Symbols give PROLITH SRM results, the solid lines show the prediction of Eq. (25).

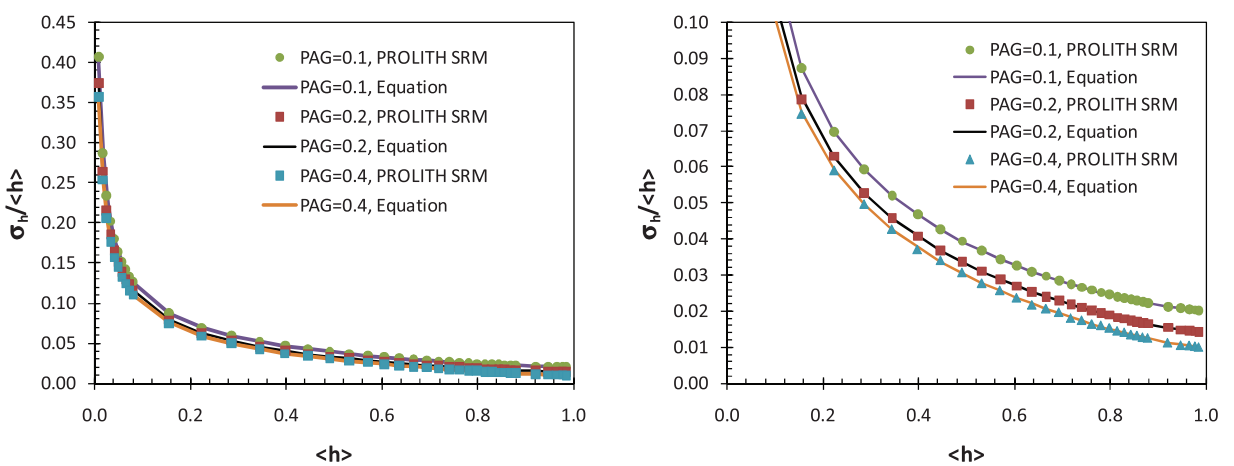

Fig. 12 Impact of initial PAG loading (with values of 0.1, 0.2, and 0.4 nm^{-3}) on the relative uncertainty in acid concentration. Symbols give the PROLITH SRM simulation results, the solid lines show the prediction of Eq. (25). The two figures differ only in the scale of the *y*-axis.

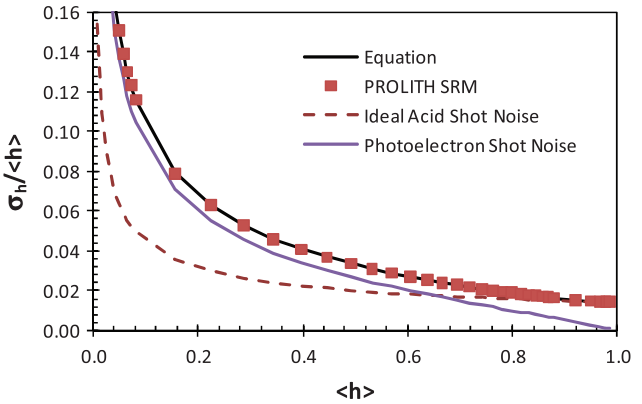

Fig. 13 For the nominal parameters of Table 2, the simulated relative acid uncertainty along with the two components of uncertainty, as defined in Eqs. (24) and (30).

the PROLITH Stochastic Resist Model are very valuable tools for making such predictions, for both the open-frame exposure test case employed in this work and the more general case of full EUV imaging. Additionally, this paper has proposed and validated analytical equations to predict mean and standard deviation of the acid concentration by matching to the PROLITH SRM. The advantage of the analytical expressions is their compactness and the intuitive way in which they point to optimization.

Consider the following important optimization question: given a certain exposure dose and a certain resist thickness, what can be done to reduce the relative uncertainty in the resulting acid concentration at the end of exposure? From Eq. (24), the options are limited:

- Increase the value of C, thus increasing $\langle h \rangle$.
- Increase α (which increases C and thus $\langle h \rangle$, but also increases $\langle n_{\text{photoelectrons}} \rangle$).
- Increase ϕ_e (which increases both $\langle h \rangle$ and $\langle n_{\text{photoelectrons}} \rangle$).
- Increase the PAG loading, $\langle n_{0-\text{PAG}} \rangle$.

These are the only approaches for reducing the relative acid concentration uncertainty for an EUV resist with a photoelectron exposure mechanism of the type modeled here. Of course, Eq. (14) details how each of the individual EUV resist parameters affect the value of the exposure rate constant C. Translating these modeling parameter goals into resist formulations, however, is challenging. The analytical expressions for C [Eqs. (14) or (21)] and for the relative acid uncertainty $\sigma_h/\langle h \rangle$ [Eq. (24)] provide quantitative predictions of how much improvement will result from a given change in one of the relevant parameters.

The state-of-the-art in EUV resist design today is based on chemically-amplified systems with polymer-bound-PAGs.[17–21] These resists are capable of 22-nm half-pitch resolution with linewidth roughness (LWR) of 4.2 nm using a sizing dose of 11 mJ/cm^2 and a 0.30 NA, dipole illumination exposure tool. At the expected dose requirements of no more than 15 mJ/cm^2, LWR remains the most difficult challenge, especially when coupled with continued reductions in feature size. However, based in part on our understanding of the EUV reaction mechanism discussed here, we can improve EUV resists using several approaches:

- Increase resist absorption of EUV light.
- Reduce the electron affinity of the matrix polymer (reduce electron energy loss that does not result in PAG excitation, thus increasing d_e and C).
- Increase the electron affinity (and thus the reaction cross-section) of the PAG.
- Minimize electron blur by increasing resist atomic density (thus reducing r_e).
- Minimize acid diffusivity by using lower activation energy leaving groups and reduced post-exposure bake temperatures.
- Reduce the spatial distribution fluctuations of PAG in the resist.
- Reduce resist sensitivity to out-of-band radiation.

EUV resist development is still at an early stage. Due to the photospeed constraints placed on EUV resists, a nonchemically amplified resist approach is not practical. Fortunately, there are a number of unique resist levers arising out of the EUV reaction mechanism which provide an opportunity to improve EUV chemically amplified resists.

6 Conclusions

When based on defensible and calibratable statistical-mechanical models, Monte Carlo approaches to simulating the stochastic nature of photoresist exposure (such as the PROLITH SRM) are extremely valuable. Such simulators are also an invaluable tool to help find simple, analytical formulas that can describe the basic stochastic behavior of resists. For 193 nm and related resists, the mechanism of exposure is simple enough that such analytical formulas can be derived from first principles. For EUV resists, with their complicated photoelectron and secondary electron exposure mechanism, a rigorous first-principles solution seems out of reach. However, by combining these two powerful tools (analytical and Monte Carlo approaches), important insights into the stochastic nature of EUV exposure can be obtained.

A method of finding the exposure rate constant C from a stochastic simulator has been demonstrated and its accuracy validated. The EUV exposure mechanism used by the PROLITH SRM was shown to be first order (as expected). Further, the influence of each PROLITH SRM parameter on C has been detailed to the point where a simple, semiempirical expression predicts C to within about 1%. With this expression, one can conveniently predict the mean concentration of acid as a function of exposure dose. This prediction is important since the mean acid concentration is needed to predict the standard deviation of the acid concentration.

For line-edge roughness modeling, predicting the standard deviation of the acid concentration at the end of exposure is an important first step. Extensive PROLITH SRM simulations have shown that a simple and intuitive analytical expression can predict the relative standard deviation of the acid concentration quite accurately. A main advantage of this expression, besides its usefulness in an overall model for LER, is to gain insight into what resist formulation and processing changes might improve the acid concentration uncertainty, and what the magnitude of the improvement will be. Further, this

analytical model can provide a practical guideline for predicting a limit for how low LER can be made, within the paradigm of the current EUV resist exposure mechanism.

References

1. T. Kozawa and S. Tagawa, "Radiation chemistry in chemically amplified resists," *Jpn. J. Appl. Phys.* **49**, 030001 (2010).
2. T. Mulders, W. Henke, K. Elian, C. Nolscher, and M. Sebald, "New stochastic post-exposure bake simulation method," *J. Microlithogr., Microfabr., Microsyst.* **4**, 043010 (2005).
3. A. Philippou, T. Mülders, and E. Schöll, "Impact of photoresist composition and polymer chain length on line-edge roughness probed with a stochastic simulator," *J. Micro/Nanolith. MEMS MOEMS* **6**, 043005 (2007).
4. A. Saeki, T. Kozawa, S. Tagawa, H. Cao, H. Deng, and M. Leeson, "Exposure dose dependence on line-edge roughness of a latent image in electron beam/extreme ultraviolet lithographies studied by Monte Carlo technique," *J. Micro/Nanolith. MEMS MOEMS* **6**, 043004 (2007).
5. G. M. Schmid, M. D. Stewart, S. D. Burns, and C. G. Willson, "Mesoscale Monte Carlo simulation of photoresist processing," *J. Electrochem. Soc.* **151**, G155–G161 (2004).
6. H. Morita and M. Doi, "Mesoscale simulations of line-edge structures based on polymer chains in development and rinse processes," *J. Micro/Nanolith. MEMS MOEMS* **9**, 041213 (2010).
7. F. H. Dill, W. P. Hornberger, P. S. Hauge, and J. M. Shaw, "Characterization of positive photoresist," *IEEE Trans. Electron Devices* **22**(7), 445–452 (1975).
8. C. A. Mack, "Absorption and exposure in positive photoresist," *Appl. Opt.* **27**(23), 4913–4919 (1988).
9. J. Biafore, M. Smith, E. Setten, T. Wallow, P. Naulleau, D. Blankenship, S. Robertson, and Y. Deng, "Resist pattern prediction at EUV," *Proc. SPIE* **7636**, 76360R (2010).
10. M. Dapor, M. Clappa, and W. Fichtner, "Monte Carlo modeling in the low-energy domain of the secondary electron emission of polymethylmethacrylate for critical-dimension scanning electron microscopy," *J. Micro/Nanolith. MEMS MOEMS* **9**, 023001 (2010).
11. P. W. Atkins, *Physical Chemistry*, 4th Ed., pp. 845–849, W. H. Freeman and Company, New York (1990).
12. K. J. Laidler, *Chemical Kinetics*, 3rd Ed., pp. 212–222, Harper Collins, New York (1987).
13. G. Han and F. Cerrina, "Energy transfer between electrons and photoresist: Its relation to resolution," *J. Vac. Sci. Technol. B* **18**(6), 3297–3302 (2000).
14. C. A. Mack, *Fundamental Principles of Optical Lithography: The Science of Microfabrication*, pp. 195–197, J. Wiley & Sons, London (2007).
15. C. A. Mack, *Fundamental Principles of Optical Lithography: The Science of Microfabrication*, p. 245, J. Wiley & Sons, London (2007). An error in the first and second printing of this book gives a slightly incorrect version of equation (6.70) on page 245. The error is corrected when the equation is reproduced in this paper.
16. C. Mack, "A Simple Model of Line-Edge Roughness," *Future Fab International* **34**, 64–76 (2010).
17. J. W. Thackeray, R. A. Nassar, R. Brainard, D. Goldfarb, T. Wallow, Y. Wei, J. Mackey, P. Naulleau, B. Pierson, and H. H. Solak, "Chemically amplified resists resolving 25 nm 1:1 line-space features with EUV lithography," *Proc. SPIE* **6517**, 651719 (2007).
18. J. W. Thackeray, R. A. Nassar, K. Spear-Alfonso, R. Brainard, D. Goldfarb, T. Wallow, Y. Wei, W. Montgomery, K. Petrillo, O. Wood, C.-S. Koay, J. Mackey, P. Naulleau, B. Pierson, and H. Solak, "Pathway to sub-30 nm resolution in EUV lithography," *J. Photopolym. Sci. Technol.* **20**(3), 411–418 (2007).
19. M. Thiyagarajan, K. Dean, and K. Gonsalves, "Improved lithographic performance for EUV resists based on polymers with photoacid generators in the backbone," *J. Photopolym. Sci Technol.* **18**(6), 737–741 (2005).
20. R. D. Allen, P. J. Brock, Y.-H. Na, M. H. Sherwood, H. D. Truong, G. M. Wallraff, M. Fujiwara, and K. Maeda, "Investigation of polymer-bound PAGs: Synthesis, characterization and initial structure/property relationships of anion-bound resists," *J. Photopolym. Sci. Technol.* **22**(1), 25–31 (2009).
21. J. Han, J. H. Oh, H. S. Joo, H. S. Lim, S. D. Cho, J. B. Shin, S. J. Park, and D. C. Seo, "Studies of acid diffusion of anionic or cationic polymer bound PAG," presented at *EUV Symposium 2010*, Chiba, Japan (2010).

Chris A. Mack developed the lithography simulation software PROLITH and founded and ran the company FINLE Technologies for 10 years. He then served as vice president of Lithography Technology for KLA-Tencor for five years, until 2005. In 2003, he received the SEMI Award for North America for his efforts in lithography simulation and education, and in 2009 he received the SPIE Frits Zernike Award for Microlithography. He is also an adjunct faculty member at the University of Texas at Austin. Currently, he writes, teaches, and consults on the field of semiconductor microlithography in Austin, Texas.

James W. Thackeray has been instrumental in the development of numerous photoresist and antireflective coating materials for ultraviolet (UV), deep-UV, and extreme UV (EUV) lithography. Currently, he leads development of the next generation of EUV resist materials for Dow Electronic Materials. He is a member of the American Chemical Society (ACS) as well as a member of the Polymeric Materials Science Engineering Division of ACS, and is a senior member of SPIE.

John J. Biafore started work in the field of optical lithography R&D in 1991. After 15 years working in the areas of photoresist design and characterization, he Joined KLA-Tencor, where he currently works as a research scientist in the FINLE division, developers of PROLITH lithography modeling software. His current interests include stochastic modeling of resists and optical lithography processes.

Mark D. Smith received his Bachelor of Science degree in chemical engineering at the University of Texas at Austin in 1994. In 2000, he received his Ph.D. in chemical engineering from Massachusetts Institute Technology. Mark is currently a Research Scientist and manager of the Advanced Development group for the PROLITH at KLA-Tencor.